Article

Rapid, Solventless, Bulk Preparation of Metal Nanoparticle-Decorated Carbon Nanotubes

Yi Lin, Kent A. Watson, Michael J. Fallbach, Sayata Ghose, Joseph G. Smith Jr., Donavon M. Delozier, Wei Cao, Roy E. Crooks, and John W. Connell

ACS Nano, **Article ASAP** • DOI: 10.1021/nn8009097 • Publication Date (Web): 11 March 2009

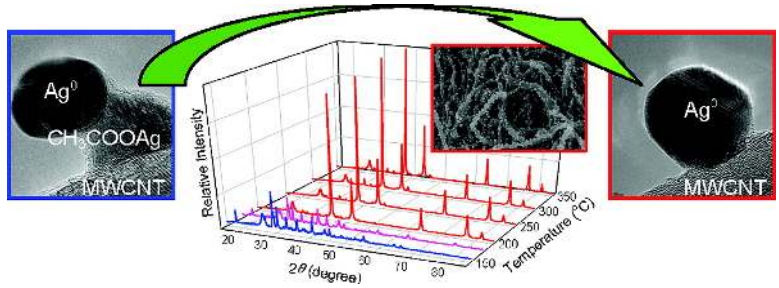

More About This Article

Additional resources and features associated with this article are available within the HTML version:

- Supporting Information
- Access to high resolution figures
- Links to articles and content related to this article
- Copyright permission to reproduce figures and/or text from this article

View the Full Text HTML

Rapid, Solventless, Bulk Preparation of Metal Nanoparticle-Decorated Carbon Nanotubes

Yi Lin,[†,¶,*] Kent A. Watson,[‡] Michael J. Fallbach,[†] Sayata Ghose,[‡] Joseph G. Smith, Jr.,[§] Donavon M. Delozier,[‡] Wei Cao,[∥] Roy E. Crooks,[‡] and John W. Connell[§,*]

[†]NASA Postdoctoral Program Fellow, NASA Langley Research Center, Hampton, Virginia 23681-2199, [‡]National Institute of Aerospace, 100 Exploration Way, Hampton, Virginia 23666-6147, [§]Mail Stop 226, Advanced Materials and Processing Branch, NASA Langley Research Center, Hampton, Virginia 23681-2199, and [∥]Applied Research Center, Old Dominion University, 12050 Jefferson Avenue, Newport News, Virginia 23606. [¶]Currently associated with National Institute of Aerospace.

ABSTRACT A rapid, solventless method is described for the decoration of carbon nanotubes with metal nanoparticles. The straightforward two-step process utilizes neither reducing agents nor electric current and involves the dry mixing of a precursor metal salt (*e.g.*, a metal acetate) with carbon nanotubes (single- or multi-walled) followed by heating in an inert atmosphere. The procedure is scalable to multigram quantities and generally applicable to various other carbon substrates (*e.g.*, carbon nanofiber, expanded graphite, and carbon black) and many metal salts (*e.g.*, Ag, Au, Co, Ni, and Pd acetates). As a model system, Ag nanoparticle-decorated carbon nanotube samples were prepared under various mixing techniques, metal loading levels, thermal treatment temperatures, and nanotube oxidative acid treatments. These nanohybrids were characterized by a variety of microscopic and spectroscopic techniques. For example, X-ray diffraction and scanning electron microscopy indicated that the average size of the Ag nanoparticles has little to do with the thermal treatment temperature but can be easily controlled by varying the Ag loading. Raman spectroscopy illustrated both the metal—nanotube electronic interactions and the surface enhancement effect from the Ag nanoparticle attachment. High-resolution transmission electron microscopy captured the *in situ* salt-to-metal conversion events on the nanotube surface. The mechanistic implications from the characterization results are discussed.

KEYWORDS: carbon nanotubes · metal decoration · nanohybrids · solventless · bulk preparation

Compared to metal and semiconductor nanoparticles, single-walled (SWCNTs) and multi-walled carbon nanotubes (MWCNTs) are considered one-dimensional nanomaterials due to their large aspect ratios that provide them with a unique combination of mechanical, electrical, and thermal properties.[1] Among the abundant carbon nanotube chemistry developed in the past decade,[2] the integration of one-dimensional nanotubes with zero-dimensional nanoparticles into hybrid structures has received increased attention.[3−5] These nanoparticle−nanotube hybrids often possess interesting structural, electrochemical, electromagnetic, and other properties that are not available to the respective components alone. As a result, they have been envisioned to be useful for catalysis,[6−8] hydrogen storage,[9] electronic sensor devices,[10,11] and many other unique applications.[3−5,12,13]

The first demonstration of a metal nanoparticle−carbon nanotube hybrid, also known as metal nanoparticle-decorated carbon nanotubes, was reported over a decade ago by Planeix *et al. via* the hydrogen reduction of an organic ruthenium salt in the presence of SWCNTs.[6] Since then, the preparation of such nanohybrids from metal salt precursors has usually involved the use of hydrogen[14] or using other reducing agents such as sodium borohydride[15] or ethylene glycol[16] while in solution to reduce the metal cations. Alternatively, the formation of metal nanoparticles on a carbon nanotube surface can be achieved electrochemically by applying a current through an aqueous metal salt solution with carbon nanotubes serving as one of the electrodes.[17,18]

Decoration of carbon nanotube surfaces with metal nanoparticles by metal salt reduction can also be achieved without the use of reducing agents or electric current.[19−22] For example, the low redox potential of SWCNTs resulted in the spontaneous formation of Au and Pt nanoparticles from aqueous $HAuCl_4$ and Na_2PtCl_4 solutions directly deposited on the surface of SWCNTs grown on a silica substrate.[19] However, most other metal cations (*e.g.*, Ag^+, Ni^{2+}, and Cu^{2+}) have lower redox potentials compared to SWCNTs and thus could not be directly reduced. To overcome this problem, Qu *et al.* reported a somewhat more complex experimental setup in which the nanotube network was supported on a metal substrate with a much lower redox potential, such as Cu or Zn.[20,21] The nanotube network served as a conductive

*Address correspondence to yi.lin-1@nasa.gov, john.w.connell@nasa.gov.

Received for review December 30, 2008 and accepted February 24, 2009.

Published online Xxxxxxxxx 00, 0000
10.1021/nn8009097 CCC: $40.75

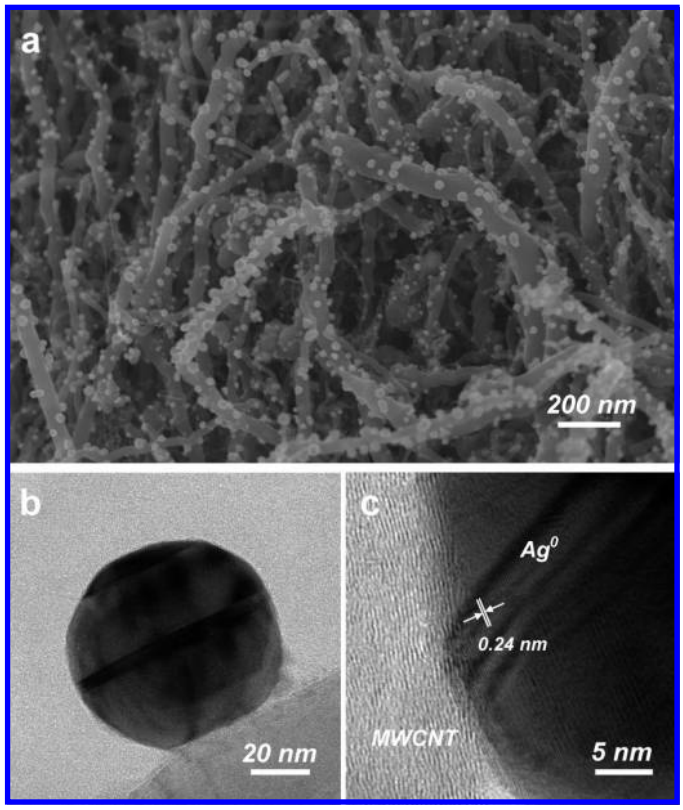

Figure 1. (a) SEM and TEM images at (b) lower and (c) higher magnifications of a Ag nanoparticle-decorated MWCNT sample with 1 mol % Ag loading.

channel with the contacting metal support underneath serving as the actual electron source, making possible the spontaneous nanoparticle formation of a far larger variety of metals on the nanotube surface.

Thermal decomposition, sometimes called pyrolysis, of metal salts has also been used extensively for the preparation of metal-containing nanoparticles and nanorods.[23−28] To obtain particles in nanometer sizes, salt decomposition was often performed at a slow heating rate and/or in a solvent.[23] Reports on the direct salt decomposition in the presence of nanosized substrates[29−31] (including carbon nanotubes[32−35]) for the preparation of metal−substrate nanohybrids, however, have been quite scarce. In this paper, a rapid, solventless, and readily scalable method to prepare various metal nanoparticle-decorated carbon nanotubes from the thermal decomposition of metal acetate/carbon nanotube solid mixtures without the use of any reducing agent is described.[36] Compared to most of the synthetic strategies available in the literature, this simple but effective "mix-and-heat" method has the advantages of many of those combined. The procedure was successfully applied to carbon nanotubes and various other carbon substrates with the use of many different metal acetates. As a model system, Ag nanoparticle-decorated carbon nanotube samples were prepared by heating mixtures of silver acetate and carbon nanotubes in an inert atmosphere. The

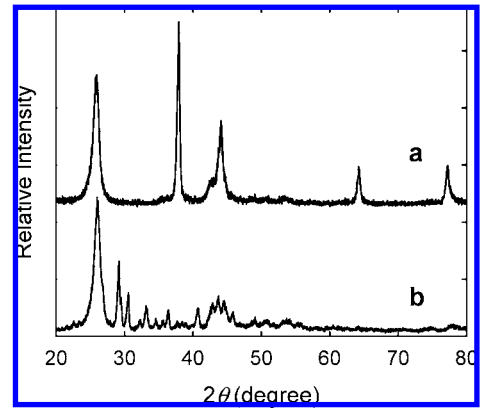

Figure 2. XRD patterns of (a) a Ag nanoparticle-decorated MWCNT sample (1 mol % Ag loading, manual mixing) and (b) the CH_3COOAg/MWCNT mixture before thermal treatment.

Ag−nanotube hybrid products from various combinations of mixing techniques, metal loading levels, thermal treatment temperatures, and nanotube oxidative acid treatments were characterized and evaluated to elucidate the synthetic mechanisms.

RESULTS AND DISCUSSION

Ag Nanoparticle-Decorated Carbon Nanotubes. The formation of metal nanoparticles on the carbon nanotube surface was achieved in a straightforward "mix-and-heat" process in the absence of any solvent, reducing agent, or electric current. In the procedure, carbon nanotubes and metal acetate powders were first manually mixed at room temperature *via* a mortar and pestle. Upon heating the acetate/nanotube mixture in a nitrogen atmosphere above the salt decomposition temperature, the metal acetate (*e.g.*, CH_3COOAg) converted into the corresponding metal (*e.g.*, Ag) and formed nanoparticles on the surface of the carbon substrates.

An SEM image of a Ag−MWCNT nanohybrid with ~1 mol % Ag loading (or ~9 wt %) is shown in Figure 1a. The average size of the Ag nanoparticles was ~47 nm. A TEM image of the sample showed the close proximity of the Ag nanoparticle and the nanotube surface (Figure 1b). The flat interface indicates that the Ag nanoparticles were grown using the nanotube surface as the template rather than by loose attachment after nanoparticle growth. At higher resolution, the Ag(111) phase (*d* spacing ~ 0.24 nm) was readily observed for the nanoparticles decorated on MWCNTs (Figure 1c).

XRD investigations (and also data from X-ray photoelectron spectroscopy (XPS); see Figure S1 in Supporting Information) confirmed the 0-valence nature of the Ag nanoparticles. As shown in Figure 2, the XRD spectrum of a starting CH_3COOAg/MWCNT mixture exhibited typical patterns from the acetate (JCPDS 14-0733), while that of the same sample after thermal treatment showed signature patterns of Ag metal (JCPDS 04-0783) at 38.0, 44.2, 64.3, and 77.2°, corresponding to the (111), (200), (220), and (311) crystal planes of Ag^0, respec-

tively. The lack of any remaining acetate diffraction patterns in the spectrum of the final nanohybrids also suggests that the salt-to-metal conversion was essentially complete. The peak at 26°, corresponding to the (002) MWCNT graphitic sidewall, exhibited little intensity change before and after the thermal treatment, suggesting the nanotube structure was well preserved.

The preparation method is highly scalable. For example, CH_3COOAg and MWCNTs with a total weight of ~10 g (1 mol % Ag loading) was mixed and heated in the same procedure except that a larger container (packed to 3 cm tall in a 100 mL glass beaker) was used for the thermal treatment. The result showed no significant difference from those obtained with much smaller batches (~100 mg in total weight). The Ag nanoparticle-decorated MWNTs were also successfully synthesized at 100 g scale using a similar procedure, suggesting the even greater scalability potential of the reported method.

***In Situ* Observation of Salt-to-Metal Conversion on MWCNT Surface.** In order to investigate the formation process of the Ag nanoparticles on the MWCNT surface, microscopy investigations were carried out on samples prepared close to the salt decomposition threshold temperature (~150 °C). While there was a significant presence of multicrystalline Ag nanoparticles for a manually mixed CH_3COOAg/MWCNT sample upon full conversion (treated to 250 °C or above; see the Effect of Thermal Treatment Temperature section), the same sample heated to only 150 °C showed a predominance of many sub-10-nm "dual-crystal"-like structures scattered on the MWCNT surfaces (Figure 3). Although Ag nanostructures were reported to be able to sinter at this temperature,[37,38] the observed "intermediate" species were not two sintering Ag nanoparticles. Rather, as shown in the high-resolution TEM (HR-TEM) image (Figure 3b), only part of the nanostructure was metallic Ag, as the crystalline lattices could be attributed to (111) (d ~ 0.23 nm) or (200) phases (d ~ 0.20 nm) of Ag^0. The rest of the dual-crystal nanostructure, however, was instead the nanocrystalline phase of CH_3COOAg (d ~ 0.30 nm).

There were two types of morphologies for the CH_3COOAg/Ag^0 dual-crystals found in samples heated to 150 °C. One is shown in Figure 3b, where both CH_3COOAg and Ag^0 phases were in contact with the nanotube surface (the droplet -type). The "mushroom"-type is shown in Figure 4, and only the CH_3COOAg phase is in contact with the nanotube surface while the Ag^0 phase is at the tip of the salt crystal. This morphology suggests that the first formation of the Ag phase started away from the nanotube surface. Upon electron beam irradiation in TEM (mimicking the further heating of the bulk sample to a higher temperature), the CH_3COOAg phase gradually collapsed upon decomposition, while the Ag^0 phase grew larger from top down and eventually attached to the nanotube surface. At this time, the salt fully converted into the metal, and no residual CH_3COOAg phase could be found (see Figure 4 and Video S1 of the conversion process in Supporting Information).

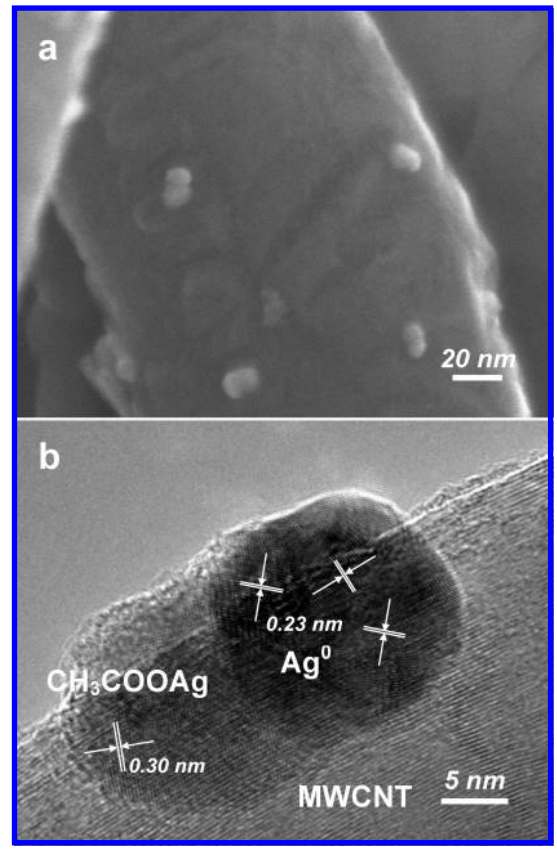

Figure 3. (a) SEM and (b) HR-TEM images of the dual-crystal species decorated on MWCNTs from a CH_3COOAg/MWCNT sample (1 mol % Ag loading, manual mixing) after thermal treatment at 150 °C. The species in the HR-TEM image is designated as the "droplet"-type.

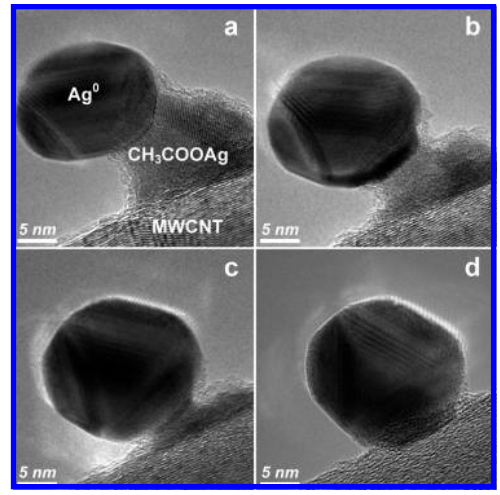

Figure 4. Progressive HR-TEM images of a mushroom-type dual-crystal from a CH_3COOAg/MWCNT sample (1 mol % Ag loading, manual mixing) after thermal treatment at 150 °C. The images were taken after approximately (a) 1, (b) 3, (c) 7, and (d) 10 min of electron irradiation on the dual-crystal.

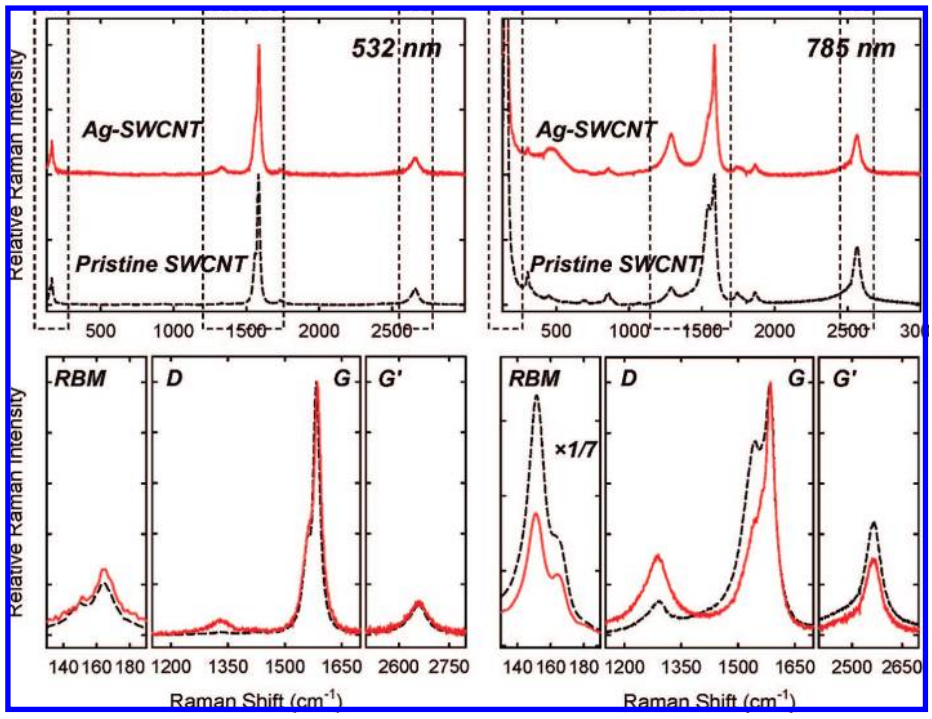

Figure 5. Full (top) and magnified regions (bottom) of Raman spectra of a Ag nanoparticle-decorated SWCNT sample (1 mol % Ag loading, manual mixing) (red solid line) and pristine SWCNTs (black dashed line).

Since carbon nanotubes are known for their reduction capability in the formation of some metal nanoparticles in solution,[19,22] it was of interest to investigate if it was also true in the thermal transformation of metal acetate to 0-valence metal. The observations here for salt-to-metal transformation of the mushroom-type intermediate CH_3COOAg/Ag^0 dual-crystals strongly indicated that the nanotube carbons did not chemically participate in the transformation because of physical distance between the nanotube and the newly formed Ag phase. This observation is consistent with the findings (*vide infra*) that even chemically inert substrates could be used to support the formation of Ag nanoparticles. On the other hand, the salt-to-metal transformation upon electron beam irradiation was also captured by HR-TEM for the droplet-type CH_3COOAg/Ag^0 dual-crystal (see Video S2 in Supporting Information), where the decomposition of the salt did occur at close proximity to the nanotube surface. In this configuration, it is possible that the nanotube carbons did chemically participate in the reaction by reducing the activation energy for the decomposition of the acetate. This will require more detailed investigations in future studies.

Raman Spectroscopy on Ag−Carbon Nanotube Interactions. Although the interaction between Ag nanoparticles and carbon nanotubes is likely *via* van der Waals forces, microscopy studies suggest that many Ag nanoparticles were still attached to the nanotube surface after a brief sonication of the nanohybrids in a solvent. Nevertheless, the physical proximity of the metal nanoparticles to the nanotubes is expected to alter the electronic transitions of the nanotubes, which can be probed *via* Raman spectroscopy. Compared to MWCNTs, SWCNTs are more suitable for spectroscopic studies due to their more distinctive spectral characteristics.

It is now well-established that excitation within the proximity of the electronic transitions of SWCNTs of certain chiralities (or metallic/semiconducting characteristics) results in resonantly enhanced Raman signals.[39] Thus by studying the Raman spectra of a given SWCNT sample at various excitation wavelengths, one can selectively probe the electronic information of a certain group of SWCNTs in the sample. According to the electronic transition−diameter dependence plot (also known as the Kataura Plot[40]), Raman excitation at 785 nm (1.58 eV) mainly probes the metallic SWCNTs in the sample (resonant with the M_{11} transition), while excitation at 532 nm (2.33 eV) selectively probes the semiconducting SWCNTs (resonant with the S_{33} transition) for the nanotubes used in this study ($d \sim 1.5$ nm).

Raman spectra obtained with excitations at 532 and 785 nm (Figure 5) of a Ag−SWCNT nanohybrid with ~1 mol % Ag loading showed features typical of SWCNTs, including the G-band (~1584 cm^{-1} at both excitations), D-band (~1330 and ~1290 cm^{-1}, respectively), G′-band (~2659 and ~2564 cm^{-1}, respectively), and the radial breathing mode (RBM) peaks (~150, 164 cm^{-1} and ~151, 165 cm^{-1}, respectively).

Compared to those of pristine SWCNTs, the G-band, G′-band, and RBM peaks of the nanohybrids exhibited little change at 532 nm excitation. This indicated that there was insignificant electronic interaction between Ag nanoparticles and semiconducting SWCNTs. At 785 nm excitation, where mainly metallic SWCNTs are in resonance, however, the relative peak intensities and line shapes underwent significant changes.

It is known that the G-band of metallic SWCNTs exhibits an unsymmetrical Breit−Wigner−Fano (BWF) line shape appearing as a shoulder to the main symmetrical Lorenzian feature.[41,42] Since the 785 nm excitation is mainly in resonance with the metallic SWCNTs, the BWF line shape was prominent in the spectrum of the pristine SWCNTs. However, with 1 mol % Ag loading, this unsymmetrical feature greatly diminishes, strongly suggesting the electronic structures of metallic SWCNTs in the sample were disturbed by the attachment of Ag nanoparticles. Such a reduction was previ-

ously reported in the p-doping of metallic SWCNTs, in which electrons are depleted from the nanotubes by the dopants.[43−46] During the preparation of this paper, similar phenomena were reported in the doping of SWCNTs with Au species.[49,50]

Consistent with the electron depletion from metallic SWCNTs by the attached Ag nanoparticles was the observation of the decrease in RBM and G′-band signal intensities relative to the G-band. The decrease of RBM signal intensities in the Ag−SWCNT nanohybrid may indicate that fewer (metallic SWCNT) species were in resonance at the given excitation wavelength (785 nm). The G′-band intensity decrease (see $I_{G'}/I_G$ values in Table S1 in Supporting Information) has been related to the decrease in the metallic character of the sample.[50,51] It should be noted that both electron and hole doping of SWCNTs are sometimes accompanied by spectral shifts of G- and/or G′-bands at appropriate conditions.[52] However, no significant shift was observed for the Ag−SWCNT samples studied in this work.

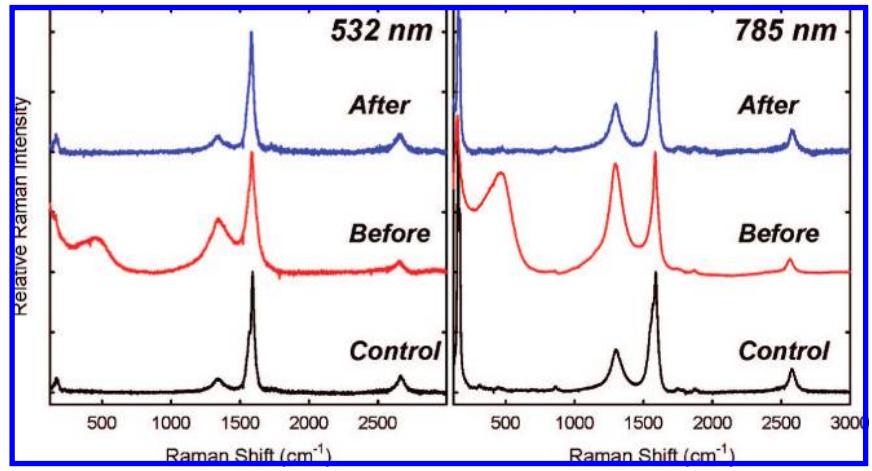

Figure 6. Raman spectra of a Ag nanoparticle-decorated SWCNT sample (50 mol % Ag loading, manual mixing) before (middle, red) and after (top, blue) refluxing with 2.6 M nitric acid for 1 h to remove Ag. The spectra of pristine SWCNTs after similar acid treatment as controls (bottom, black) are shown for comparison.

Another obvious change in the spectra at both 532 and 785 nm excitations shown in Figure 5 was the substantial increase of the SWCNT D-band with Ag loading (see I_D/I_G values in Table S1 in Supporting Information). Since the D-band is known to be related to nanotube defects, such an increase is often attributed to the direct functionalization of the nanotube conjugated sidewall with the aromatic carbons being converted to an sp^3 hybridization.[2] To determine if the nanotube sidewall was indeed damaged (*i.e.*, change of hybridization from sp^2 to sp^3) upon Ag attachment, a Ag nanoparticle-decorated SWCNT sample with 50 mol % Ag loading (and thus a very prominent D-band) was refluxed in 2.6 M HNO_3 for 1 h to dissolve the Ag nanoparticles. As shown in Figure 6, the D-band of the same sample after acid treatment significantly decreased, with the spectrum almost identical to that of a control SWCNT sample after the same treatment. Since the use of nitric acid could only bring more defects to the nanotubes,[2] the observed reversibility of the D-band intensity strongly suggests that the signal increase was *not* due to any permanent damage of the nanotube sidewall structure from the attachment of Ag nanoparticles.

Ag is a well-known metal for surface-enhanced Raman spectroscopy (SERS).[53,54] In SERS, due to the close proximity of the target molecules and metal surface, the Raman signals of the target are enhanced by the surface plasmon of the metal. Although the structural distortion (rather than damage) of the SWCNT conjugate surface upon Ag decoration might lead to some D-band intensity increase, the dominant mechanism for the above observation should be that the Ag nanoparticle preferentially attached adjacent to the intrinsic defect sites on the SWCNT surface, thus providing a selective surface-enhancement effect of the defect-induced Raman signal (*i.e.*, D-band).[55]

The overall SERS spectral intensity enhancement (G-band, G′-band, and RBM) was rather insignificant possibly because of the intrinsic resonance effect of SWCNTs.[56−58] MWCNTs, on the other hand, exhibit less resonance effects, and the overall SERS enhancement factors were much higher (*e.g.*, G-band intensity increased ~10 times at 10 mol % Ag loading; see Figure S2 in Supporting Information). Interestingly, and similar to SWCNTs, the D-band enhancement of MWCNTs seemed to also be higher relative to the G-band with the increase of Ag loading, suggesting a similar selective local SERS effect.

In addition to the major SWCNT peaks discussed above, there was also a prominent feature that appeared at ~470 cm^{-1} for the Ag−SWCNT nanohybrids at both 532 and 785 nm excitations (Figures 5 and 6). This peak was found to increase with the Ag loading and disappeared after the previously discussed Ag removal experiment. Although the exact origin of the feature is currently not well understood, the correlation of its trend to the D-band intensity change seems to suggest that it was also due to the SERS effect of some less prominent nanotube Raman modes upon Ag attachment. Several of the so-called intermediate frequency modes (IFM) of SWCNTs are located in this spectral region.[59−61]

Mechanical Mixing *via* Ball-Milling. Compared to simple manual mixing with a mortar and pestle, mechanical mixing using commercially available ball-milling equipment might afford a more efficient mixing of the metal salts with carbon nanotubes and hence improve the reproducibility. Figure 7 shows an SEM image of the

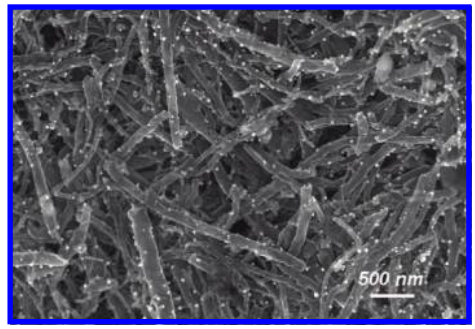

Figure 7. SEM image of a Ag nanoparticle-decorated MWCNT sample with ~1 mol % Ag content prepared *via* ball-milling process.

sample prepared *via* ball-milling the CH_3COOAg/MWCNT mixture followed by the same thermal treatment described earlier. Similar to the manually mixed samples, the Ag nanoparticles were well distributed on the MWCNT surface. Compared to the manually mixed nanohybrid of similar Ag loading (~1 mol %, Figure 1), however, the Ag nanoparticles decorated on the MWCNTs were of a smaller average particle size (~28 nm). The reduction in the average nanoparticle size is likely due to a more aggressive mixing *via* ball-milling, which increased the available nanotube surface area and/or the number of active anchoring/growth sites such as defects. Prolonged ball-milling causes damage to the carbon nanotube structure;[62−64] therefore, short milling time of ≤10 min was used. Under this condition, MWCNTs were moderately shortened from tens of micrometers to a few micrometers (Figure 7).

Effect of Metal Loading. A general observation during the experiments of varying Ag loadings was that the average size of Ag nanoparticles increased with higher Ag content from either manual or mechanical mixing. For example, the average Ag nanoparticle size was ~47 nm for the 1 mol % Ag−MWCNT nanohybrid sample from manual mixing (Figure 1), whereas those of ~4 and ~7 mol % loadings showed average particle sizes of ~64 and ~81 nm, respectively (Figure 8). Theoretically, if the total particle number is constant, the Ag content (C_{Ag}) should be proportional to the average volume (V_{Ag}) of Ag nanoparticles, which our results seemed to corroborate (Figure S3 in Supporting Information). This suggests a rather consistent number of nanoparticle anchoring/growth sites on the carbon nanotube surface in spite of the metal loading level. Therefore, under similar preparation conditions, the average size of Ag nanoparticles decorated on MWCNTs could be conveniently predicted and controlled by simply varying the Ag loading.

The SEM images of Ag nanoparticle-decorated SWCNTs of several Ag loadings from manual mixing are shown in Figure 9. The average size of Ag nanoparticles decorating SWCNTs was generally smaller than that of MWCNTs with the same Ag loading, which was likely due to the higher surface area of SWCNTs. Nevertheless, the images clearly showed a similar increase of the Ag nanoparticle size with increasing Ag loading. Direct particle size measurement using SEM might be affected by the presence of catalytic particles (leftover from the production process of SWCNTs). Alternatively, UV/vis/NIR optical absorption experiments could be used for a supportive qualitative assessment. The same set of Ag nanoparticle-decorated SWCNT samples as those shown in Figure 9 (Ag contents of 5, 10, and 20 mol % from manual mixing) was dispersed in DMF using a brief bath sonication. Each of the above samples was then passed through a coarse filter and immediately placed in a quartz cuvette for the optical absorption studies. The spectra (Figure 10) showed the Ag plasmon band typical for nanosized Ag species.[65] It was found that the Ag plasmon band red-shifted from 413 to 423 nm with higher Ag loading (from 5 to 20 mol % Ag), which is consistent with the size increase of the Ag nanoparticles.[66]

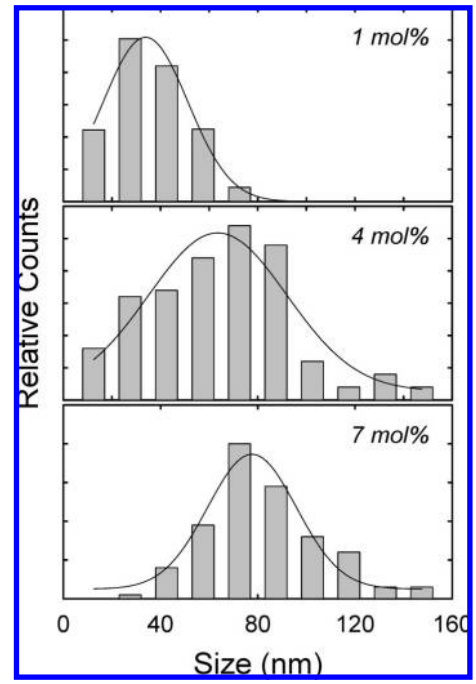

Figure 8. Size distribution plots of Ag nanoparticles in a series of Ag−MWCNT nanohybrid samples prepared *via* manual mixing.

It should be noted that the optical spectra of Ag nanoparticle-decorated SWCNTs dispersed in DMF also featured typical electronic transitions of both semiconducting and metallic SWCNTs (*i.e.*, the second semiconducting transition (S_{22}) band centered at ~1000 nm and the first metallic transition (M_{11}) band centered at ~750 nm). Compared to the spectrum of pristine SWCNTs,[67] both S_{22} and M_{11} bands appeared weaker with higher Ag loading, with the latter somewhat more affected. These observations are consistent with the electronic interactions between metallic SWCNTs and attached Ag nanoparticles revealed from the Raman results in the previous section.

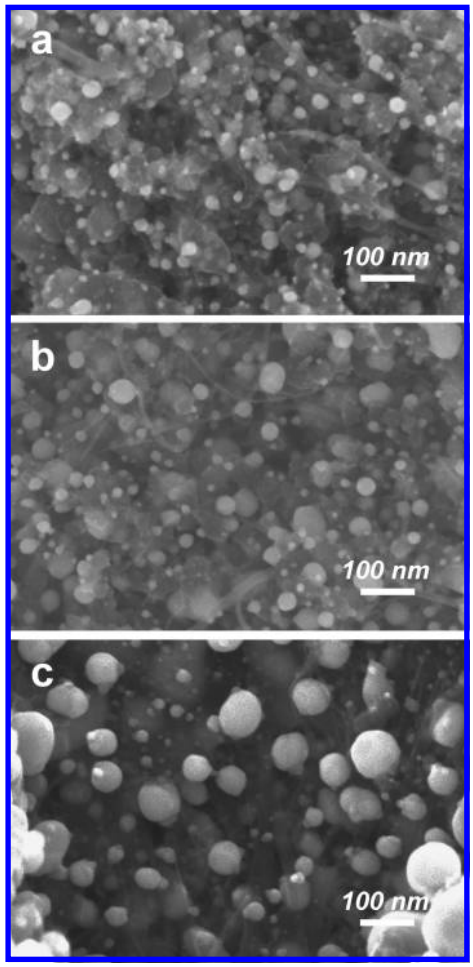

Figure 9. SEM images of Ag nanoparticle-decorated SWCNT samples with (a) 5, (b) 10, and (c) 20 mol % Ag loadings.

Effect of Thermal Treatment Temperature. The thermal decomposition temperatures were found to be ~276 °C for the as-received CH_3COOAg powder and ~250 °C for a manually mixed CH_3COOAg/MWCNT sample with 10 mol % Ag loading. This was determined from the endothermic peak of the DTG curve obtained at 5.4 °C/min in N_2 (see Figure S4 in Supporting Information). The decrease of the salt thermal decomposition temperature can be attributed to the distribution of smaller salt particles on the nanotube surface in the mixture. The thermal decomposition of the salt for a similar mixture from ball-milling occurred at an even lower temperature (~225 °C). This indicates that the salt particles were better dispersed as a result of improved mixing and perhaps more efficient heat adsorption from the proximity to thermally conductive MWCNTs. In addition, the decomposition threshold of the CH_3COOAg/MWCNT mixture was as low as ~180 °C from manual mixing and ~150 °C from mechanical mixing, suggesting that the use of lower thermal treatment temperatures (instead of 300 or 350 °C used in most of the experiments) might also be successful.

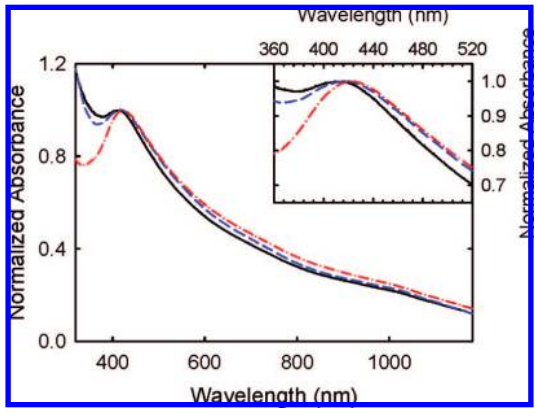

Figure 10. UV/vis/NIR spectra of Ag nanoparticle-decorated SWCNT samples with 5 (black solid line), 10 (blue dashed line), and 20 mol % (red dash-dot line) Ag loadings. The inset shows the enlarged Ag plasmon band region.

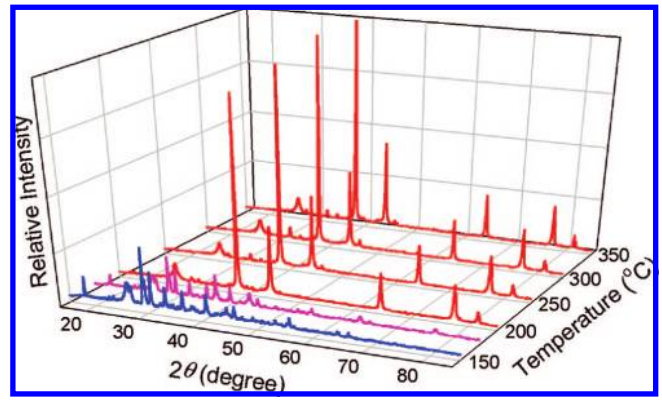

Figure 11. XRD patterns of the Ag−MWCNT nanohybrids from the same CH_3COOAg/MWCNT mixture (10 mol % Ag loading, manual mixing) heated to different temperatures.

Thus, a series of experiments were performed for CH_3COOAg/MWCNT mixtures at 1 and 10 mol % Ag loadings, with the mixtures heated to 150, 175, 200, 250, 300, and 350 °C. The heating rate was kept constant at 5.4 °C/min, and the isothermal time was adjusted so that the total thermal treatment time was constant at 100 min. Taking the results for the CH_3COOAg/MWCNT mixture from manual mixing with 10 mol % Ag loading as an example, the XRD data of the sample heated to 150 °C (Figure 11) showed characteristic peaks of CH_3COOAg (*e.g.*, $2\theta \sim 29°$) with negligible Ag^0 phase (*e.g.*, $2\theta \sim 38°$), indicating that little salt-to-metal conversion occurred at this temperature. As the thermal treatment temperature increased to 200 °C, the conversion increased dramatically as seen from the increase of the Ag^0 peaks and the concurrent decrease of the CH_3COOAg peaks in the XRD spectra. Further increase of thermal treatment temperature resulted in little spectral intensity change, suggesting the process was driven to completion.

Since the nanotube structure remained essentially unchanged after thermal treatment, the salt-to-metal conversion yields may be estimated by comparing the XRD intensity ratio of the $Ag^0(111)$ peak (~38°) to the MWCNT(002) peak (~26°) at a given thermal treatment temperature to the ratio found at 350 °C, at which the

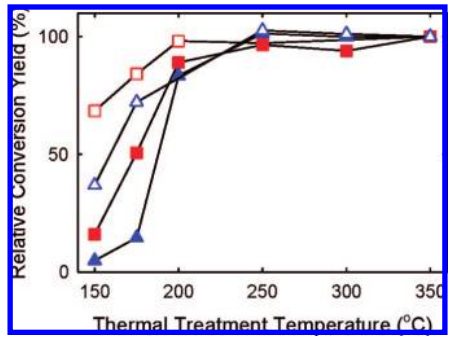

Figure 12. Relative salt-to-metal conversion yield *versus* thermal treatment temperature of the same CH_3COOAg/MWCNT mixtures: (△) 1 mol % Ag loading, manual mixing; (□) 1 mol % Ag loading, mechanical mixing *via* ball-milling; (▲) 10 mol % Ag loading, manual mixing; and (■) 10 mol % Ag loading, mechanical mixing *via* ball-milling. The yields were calculated from the intensity ratios of Ag(111) peak and MWCNT(002) peak and normalized to 100% at 350 °C. The lines are provided as aids for visualization.

complete conversion is assumed. For example, the relative conversion yield for the CH_3COOAg/MWCNT manual mixture with 10 mol % Ag loading was calculated to be ~85% when heated to 200 °C and became nearly quantitative at 250 °C and above within the experimental error (Figure 12). A similar trend was also found for the manually mixed 1 mol % Ag−MWCNT sample.

At temperatures below 200 °C, the salt-to-metal conversion yields for mechanically mixed samples *via* ball-milling were higher than those from manual mixing at the same loadings. For example, the conversion yield for a CH_3COOAg/MWCNT mixture at 1 mol % Ag loading from ball-milling was as high as ~70% when heated to 150 °C, while those from manual mixing was only ~15%. This may be partially due to the lower decomposition threshold temperature of the salt in the mechanical mixture.[68] Nevertheless, the conversions for mechanically mixed samples still reached the completion plateau at similar temperature range (200−250 °C, Figure 12).

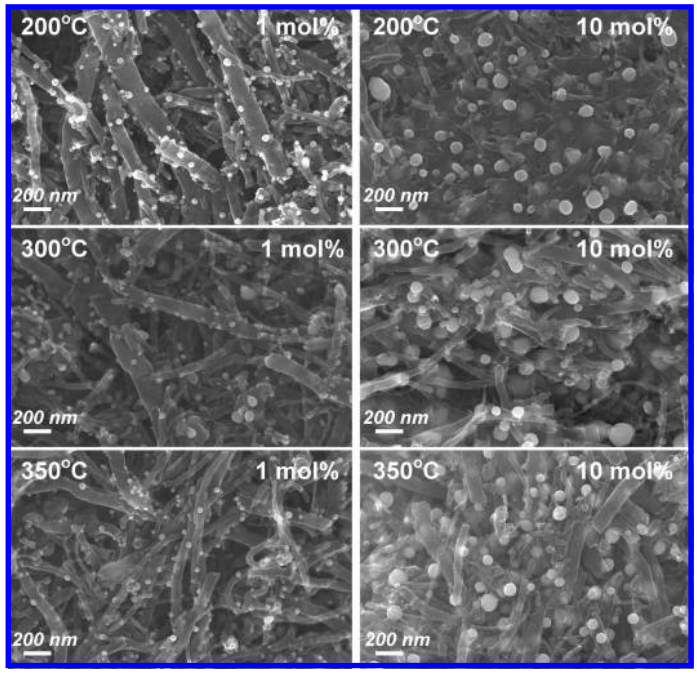

Figure 13. SEM images of two series of Ag nanoparticle-decorated MWCNTs generated using mechanical mixing and 1 (left) and 10 mol % (right) Ag loadings obtained after thermal treatment at 200 (top), 300 (middle), and 350 °C (bottom).

Analyses of SEM images of samples obtained at different thermal treatment temperatures indicated that there was little change to the average size of the Ag nanoparticles at and above 200 °C, where the salt-to-metal conversion was near completion. Shown in Figure 13 as a representative example are the mechanically mixed CH_3COOAg/MWCNT samples of 1 and 10 mol % Ag loading treated at various temperatures. The average sizes of Ag nanoparticles decorated on MWCNTs in the thermal treatment range of 200−350 °C were relatively consistent at ~30 nm for 1 mol % loading and ~70 nm for 10 mol % loading (Table S2 in Supporting Information). These results strongly suggest that the thermal treatment temperature for decomposable salts could be set slightly above their decomposition thresholds to achieve satisfactory conversion into decorated nanoparticles without significantly affecting their sizes.

Effect of Oxidative Acid Treatments. Refluxing carbon nanotubes in oxidative acids such as nitric acid is a common purification method to remove metal catalysts and some carbon impurities from the nanotube production.[2] The oxidative acid treatment induces the formation of oxygen-containing functionalities such as carboxylate groups at the nanotube end and along surface defect sites due to the oxidation of nanotube carbons. These functional groups are amenable to further modifications with various organic and inorganic compounds,[2] including the chelation of the carboxylates with solvated metal ions followed by reduction to form metal nanoparticles on the nanotube ends and surface.[69,70]

Although the above-reported results with pristine carbon nanotubes indicate that the formation of metal nanoparticles on a nanotube surface does not require the significant presence of nanotube surface-attached carboxylate functional groups, it was still interesting to investigate whether such oxidative acid treatment on the nanotube would have any prominent effect on the decoration of metal nanoparticles in this solventless process.

The treatment of pristine MWCNTs was conducted by refluxing with 70% HNO_3 for 16 h, followed by filtering and thorough washing of the material with deionized water until pH ~7. The acid-treated MWCNTs were dried in a vacuum oven and subjected to a similar "mix-and-heat" process with CH_3COOAg to afford Ag nanoparticle-decorated MWCNTs. As shown in Figure 14, the density of the nanoparticle decoration on the acid-treated MWCNTs appeared higher than that from

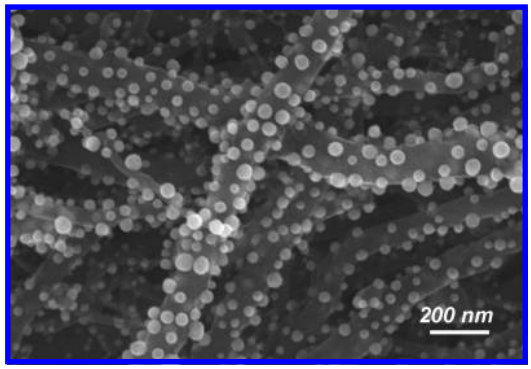

Figure 14. SEM image of a Ag nanoparticle-decorated MWCNT sample (1 mol % Ag loading, manual mixing) in which MWCNTs were pretreated with concentrated nitric acid before mixing with the acetate.

pristine MWCNTs as seen in Figure 1. In addition, the decorated Ag nanoparticles appeared more spherical with a somewhat smaller average size (~39 nm from treated MWCNTs *vs* ~47 nm from pristine MWCNTs at 1 mol % loading). This can be attributed to new defect sites generated on the nanotube surface by the oxidative acid treatment, resulting in additional nucleation centers for Ag nanoparticle growth, allowing for a denser distribution of nanoparticles and thus smaller sizes given the same total loading. Additionally, it is likely that the oxygen-containing functional groups, even in this solventless process, could lead to a more homogeneous nucleation of the forming metal nanoparticle at each anchoring site, thus making the final nanoparticles appear somewhat more spherical.

Different Substrates. The same mix-and-heat process successfully applied to both MWCNTs and SWCNTs discussed above was found to be generally applicable to various other carbon substrates, including carbon nanofibers, expanded graphite, and carbon black. As shown in Figure 15, despite the differences in average sizes and size distributions, Ag nanoparticles were formed on all of the carbon substrates investigated.[71] It was interesting to observe that the Ag nanoparticle decoration could also be achieved on Zeeospheres, silica−alumina ceramic microspheres. This result suggests that the reduction capability of the substrate is not a prerequisite for metal nanoparticle formation from thermal decomposition of metal salts, consistent with the mechanistic discussions emanating from the high-resolution TEM study in the previous section. However, the size, shape, and decorating location of the nanoparticles formed should vary according to the surface nature of the substrates.

Different Metal Acetates. To further test the general applicability of the mix-and-heat method, many other metal acetates, including gold(III), colbalt(II), copper(II), iron(II), nickel(II), lead(II), palladium(II), and zinc(II) acetates, were also used as starting materials in similar experiments with MWCNTs as the substrates.[76] In these experiments, the metal salts were manually mixed with

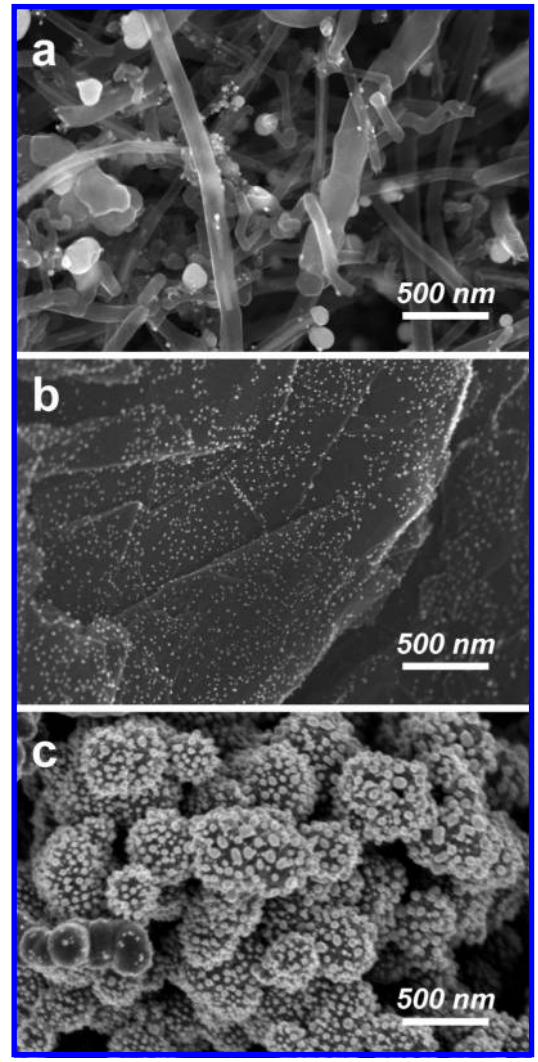

Figure 15. SEM images of Ag nanoparticle-decorated (a) carbon nanofiber, (b) expanded graphite, and (c) carbon black. The Ag loadings were all 1 mol %.

MWCNTs and heated to various temperatures from 300 to 450 °C according to the decomposition temperatures of the respective salts (Table S3 in Supporting Information).

It is known that thermal decomposition of a metal acetate usually yields the corresponding metal or metal oxide[77−80] (similar to metal nitrates[81−83]). Indeed, gold(III), cobalt(II), nickel(II), and palladium(II) acetates were found to behave similarly to CH_3COOAg, yielding the corresponding metallic nanoparticles on the MWCNT surfaces. As shown in Figure 16, the decomposition of these acetates yielded nanoparticle-decorated MWCNTs, with narrowly distributed particle sizes on the order of several to tens of nanometers (dependent upon the metal and the loading level). The metallic nature of these nanoparticles was confirmed *via* XRD (Figure S5 in Supporting Information).

Thermal decomposition of the mixtures of MWCNTs and other metal acetates, such as iron(II) and zinc(II), yielded nanohybrids with the corresponding metal ox-

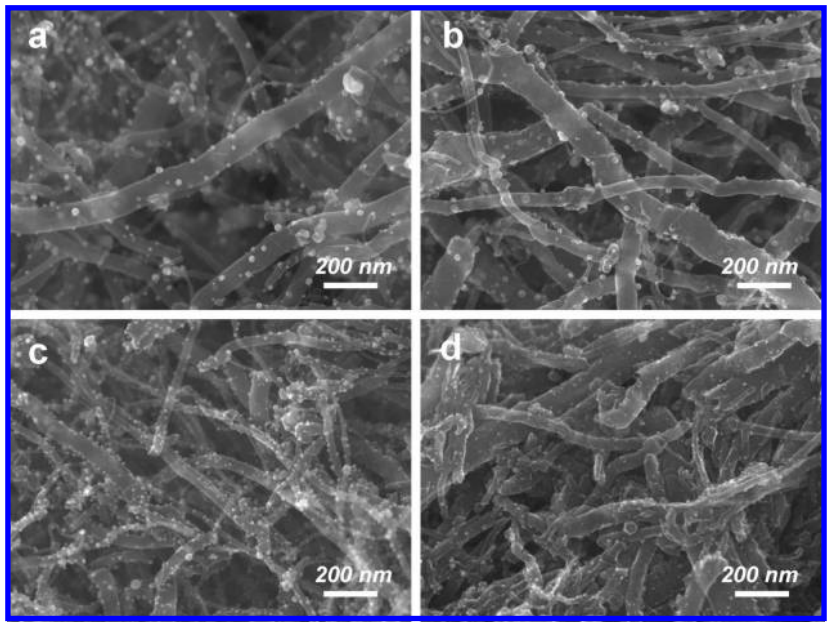

Figure 16. SEM images of MWCNTs decorated with metallic nanoparticles of (a) 10 mol % Au (manual mixing), (b) 1 mol % Co (manual mixing), (c) 10 mol % Ni (manual mixing), and (d) 1 mol % Pd (mechanical mixing *via* ball-milling).

ide nanoparticles decorating the nanotube surfaces (Figure 17 and Figure S6 in Supporting Information). It is interesting to note that while iron oxide (Fe_3O_4 or γ-Fe_2O_3) appeared as individual nanoparticles similar to the metallic nanoparticles discussed above, ZnO tended to form clusters of nanoparticles on the MWCNT surfaces at the given experimental conditions (ramped to 350 at 5.4 °C/min and held for 3 h).

Among the acetates investigated in this work, lead(II) acetate decomposed into a mixture of Pb metal and PbO with MWCNTs as the substrate. The particles formed on the nanotube surface in sizes as large as hundreds of nanometers likely because the necessary thermal treatment temperature for decomposition (>360 °C) exceeded the melting point of the Pb metal (~327 °C). Copper(II) acetate, on the other hand, did yield metallic Cu upon thermal treatment of its mixture with MWCNTs according to XRD, but micron-sized chunks with sparsely decorated nanospecies were found on the nanotube surface. The difference in the capability of nanosized particle formation on the substrates from these metal acetates may be related to the nanotube surface wettability with the corresponding metals or metal oxides.[84,85] In addition, the phase transformation of the salt itself during the thermal decomposition event may also play a significant role. For example, palladium(II) acetate is known to sublimate before it decomposes,[78] which might explain the formation of quite evenly distributed Pd^0 nanoparticles decorated on the MWCNT surfaces. It is worth noting that because of such difference in the nanoparticle formation for various metal salt precursors on a given substrate, the experimental parameters used to control the decorated particle size and distribution in the reported mix-and-heat procedure might also vary for different metal salt/substrate systems.

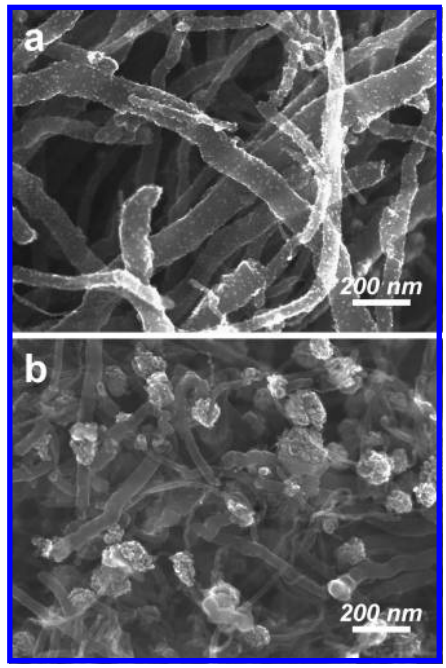

Figure 17. SEM images of MWCNTs decorated with metal oxide nanoparticles of (a) 10 mol % Fe (manual mixing) and (b) 10 mol % Zn (manual mixing).

SUMMARY

A rapid, solventless, and scalable method was reported for the preparation of Ag nanoparticle-decorated carbon nanotubes using silver acetate as the thermal decomposable precursor without the use of any reducing agent or electric current. In this procedure, the metal salt and the nanotubes were simply mixed in the solid state and heated to the thermal decomposition temperature of the salt in an inert atmosphere to produce the metal−nanotube nanohybrids.

The Ag nanoparticle-decorated MWCNTs and SWCNTs were synthesized as model systems and characterized in detail *via* instrumental techniques such as SEM, HR-TEM, XRD, Raman, and optical absorption spectroscopy. The metallic nature of the nanoparticles was confirmed by HR-TEM and XRD. The average nanoparticle size was found to be independent of thermal treatment temperature (as long as the salt-to-metal conversion was nearly complete) but increased with metal loading. The latter observation clearly indicates that there is a relatively consistent number of nanoparticle anchoring sites on the nanotube surface, making the control of nanoparticle size possible by simply varying the metal loading levels. The use of mechanical mixing or oxidative acid treatment of the starting MWCNTs pro-

vided decorated Ag nanoparticles with reduced sizes, likely due to the increased number of nanotube surface anchoring sites.

Results from resonance Raman spectra of various Ag−SWCNT nanohybrids suggest that electrons were depleted from metallic SWCNTs by Ag nanoparticles, but no electron flow could be identified with semiconducting SWCNTs. The D-band intensity increase and the new feature appearing at ~470 cm^{-1} upon Ag nanoparticle decoration were both reversible when the metal was removed and are likely due to the selective local SERS effects from the Ag nanoparticles. The overall SERS effect of Raman signals was more pronounced for the MWCNT-based nanohybrids since less resonance effect was involved.

HR-TEM studies of a CH_3COOAg/MWCNT mixture heated to 150 °C (close to the salt decomposition threshold in the mixture) not only revealed the presence of intermediate CH_3COOAg/Ag^0 nanospecies but also visually demonstrated that the thermal decomposition of the salt could occur both on and remotely from the nanotube surface. The latter scenario strongly suggests that the reduction role of the substrate is not a prerequisite for metallic nanoparticle formation. Indeed, the reported mix-and-heat method was generally applicable to not only carbon but also chemically inert substrates such as silica−alumina ceramic microspheres.

In similar mix-and-heat processes, other metal acetates, such as those of Au, Co, Ni, and Pd, also successfully decorated the carbon nanotubes as metal nanoparticles, while the use of iron and zinc acetates yielded the corresponding metal oxide−nanotube nanohybrids. Nevertheless, the facileness, versatility, and scalability of the method should make it valuable in preparing various metal or metal oxide nanoparticle-decorated carbon and other nanostructures for catalytic, electronic, optical, or other applications. One of the examples was our recent report on such Pd nanoparticle-decorated SWCNT and EG samples, which were found to have superior mercury adsorption capabilities when used as injected sorbents.[86] Polymeric composites using the Ag nanoparticle-decorated MWCNTs as fillers are being investigated for their electromagnetic properties potentially useful for antenna applications.[87]

METHODS

Materials. MWCNTs (diameter ~ 20−150 nm) and SWCNTs (diameter ~ 1.5 nm) were obtained from University of Kentucky and Carbon Solutions, Inc., respectively. Silver(I) acetate (99%), copper(II) acetate (98%), cobalt(II) acetate (99.995%), and palladium(II) acetate (99.9+%) were purchased from Sigma-Aldrich Co. Lead(II) acetate trihydrate (99.999%), gold(III) acetate (99.99%+), nickel(II) acetate tetrahydrate (99.5%), and zinc(II) acetate dihydrate (99%) were purchased from Acros Organics, ESPICorp Inc., J.T. Baker, and Mallinckrodt, respectively. Carbon nanofibers, carbon black (Thermax Powder N-991), and expanded graphite (Grade 3775, Lot 3438) were provided by Applied Sciences, Inc., Cancarb, Ltd., and Asbury Carbons, Inc., respectively. Zeeospheres (Type 200, silica−alumina ceramic microspheres) were obtained from Zeelan Industries, Inc. All materials and chemicals were used as received unless otherwise specified.

Measurements. High-resolution scanning electron microscopy (SEM) was conducted using a Hitachi S-5200 field-emission scanning electron microscope equipped with a "through-the-lens" secondary electron detector and an energy dispersive spectrometer (EDS). Transmission electron microscopy (TEM) was conducted on JEOL 2100 field-emission or Hitachi H-9500 transmission electron microscope systems. X-ray photoelectron spectroscopy (XPS) studies were performed on a Kratos Axis 165 system. X-ray diffraction (XRD) analyses were performed on Siemens D5000 X-ray diffractometer or Scintag XDS-2000 powder diffraction system, both with Cu Kα as the radiation sources (λ = 1.5418 Å). Optical absorption spectra were obtained using a Perkin-Elmer Lambda 900 UV/vis/NIR or a Shimadzu UV-2101PC. Raman spectroscopy was performed using a Thermo Nicolet Almega dispersive Raman spectrometer with 785 and 532 nm excitation sources. Thermogravimetric (TG) and differential thermogravimetric (DTG) measurements were performed on a Seiko TG/DTA 220 (SSC/5200) system at a rate of 5.4 °C/min with a steady nitrogen flow.

Metal Nanoparticle-Decorated Carbon Nanotubes. In a typical manual mixing experiment to prepare Ag nanoparticle-decorated MWCNTs with 1 mol % Ag loading, MWCNTs (100 mg, ~8 mmol carbon equivalent) were dry mixed with powdered CH_3COOAg (13 mg, 0.08 mmol) using a mortar and pestle until homogeneous (about 10−15 min) under ambient conditions. The solid CH_3COOAg/MWCNT mixture was then transferred to a glass vial or an aluminum pan and heated in a nitrogen oven (Blue M Electric A-5245-Q Inert Gas Oven) to 300 or 350 °C over 1 h and held isothermally for 3 h. The product was then collected as the final Ag nanoparticle-decorated MWCNT nanohybrid sample.

For mechanically mixed samples prepared *via* ball-milling with the same Ag loading, MWCNTs (500 mg, ~40 mmol carbon equivalent) and CH_3COOAg (65 mg, 0.4 mmol) were added to a zirconia vial (SPEX CertiPrep, 6.4 cm long, 5.7 cm outer diameter, ~20 mL mixing load). After placing two zirconia balls (diameter = 1.3 cm) in the vial, the set was secured in a SPEX CertiPrep 8000D High-Energy Shaker Mill and subjected to mechanical shaking (~1060 back-and-forth cycles per minute, 5.7 cm back-and-forth and 2.5 cm side-to-side movements) for 10 min. The mixture obtained was subjected to the same thermal treatment process as described above to yield the final Ag−MWCNT nanohybrid product.

Such mix-and-heat procedures *via* manual or mechanical mixing were performed with various amounts of CH_3COOAg to obtain Ag−MWCNT nanohybrid products in a series of Ag loadings. The same procedures were also applied using SWCNTs as the substrate to produce Ag nanoparticle-decorated SWCNT nanohybrids.

Acknowledgment. Y.L. and M.J.F. were supported by appointments to the NASA Postdoctoral Program at the Langley Research Center, administered by Oak Ridge Associated Universities (through NASA contract NNH06CC03B) and the National Research Council, respectively. The authors thank D. Hartman for XRD experiments, T. Williams for assistance in sample preparation and particle size measurements, and Drs. P. Lillehei, A. Belcher, and C. Wohl for their valuable comments and suggestions. The authors are in debt to Prof. Y.-P. Sun and his research group at Clemson University for their generous help in microscopy and other experiments, and Dr. J. Hudson at Clemson University for XPS measurements.

Supporting Information Available: Slideshow videos showing the salt-to-metal conversion from the intermediate CH_3COOAg/Ag^0 species to Ag nanoparticles on MWCNT surfaces; XPS spec-

trum (Ag 3d region) of a Ag nanoparticle-decorated MWCNT sample; Raman spectra of Ag nanoparticle-decorated MWCNTs; a plot of Ag nanoparticle volume *vs* Ag loading; DTG curves for manual and mechanical CH_3COOAg/MWCNT mixtures; XRD patterns of various metal and metal oxide nanoparticle-decorated MWCNT samples; SEM and XRD pattern of a Pt/MWCNT nanohybrid sample; a table of Raman peak intensity ratios ($I_{G'}/I_G$ and I_D/I_G) of Ag nanoparticle-decorated SWCNT samples of various Ag loading levels; a table comparing the sizes of Ag nanoparticles in the samples from Figure 13 as directly measured by SEM *vs* estimated using the Scherrer equation; and a table of endothermic peak temperatures of various acetate salts and the respective thermal treatment temperatures used. This material is available free of charge *via* the Internet at http://pubs.acs.org.

REFERENCES AND NOTES

1. Ajayan, P. M. Nanotubes from Carbon. *Chem. Rev.* **1999**, *99*, 1787–1799.
2. Tasis, D.; Tagmatarchis, N.; Bianco, A.; Prato, M. Chemistry of Carbon Nanotubes. *Chem. Rev.* **2006**, *106*, 1105–1136.
3. Wildgoose, G. G.; Banks, C. E.; Compton, R. G. Metal Nanoparticle and Related Materials Supported on Carbon Nanotubes: Methods and Applications. *Small* **2006**, *2*, 182–193.
4. Georgakilas, V.; Gournis, D.; Tzitzios, V.; Pasquato, L.; Guldi, D. M.; Prato, M. Decorating Carbon Nanotubes with Metal or Semiconducting Nanoparticles. *J. Mater. Chem.* **2007**, *17*, 2679–2694.
5. Correa-Duarte, M. A.; Liz-Marzan, L. M. Carbon Nanotubes as Templates for One-Dimensional Nanoparticle Assemblies. *J. Mater. Chem.* **2006**, *16*, 22–25.
6. Planeix, J. M.; Coustel, N.; Coq, J.; Brotons, V.; Kumbhar, P. S.; Dutartre, R.; Geneste, P.; Bernier, P.; Ajayan, P. M. Application of Carbon Nanotubes as Supports in Heterogeneous Catalysts. *J. Am. Chem. Soc.* **1994**, *116*, 7935–7936.
7. Liu, Z.; Lin, X.; Lee, J. Y.; Zhang, W.; Han, M.; Gan, L. M. Preparation and Characterization of Platinum-Based Electrocatalysts on Multiwalled Carbon Nanotubes for Proton Exchange Membrane Fuel Cells. *Langmuir* **2002**, *18*, 4054–4060.
8. Li, W.; Liang, C.; Zhou, W.; Qiu, J.; Zhou, Z.; Sun, G.; Xin, Q. Preparation and Characterization of Multiwalled Carbon Nanotube-Supported Platinum for Cathode Catalysts of Direct Methanol Fuel Cells. *J. Phys. Chem. B* **2003**, *107*, 6292–6299.
9. Kim, H.-S.; Lee, H.; Han, K.-S.; Kim, J.-H.; Song, M.-S.; Park, M.-S.; Lee, J.-Y.; Kang, J.-K. Hydrogen Storage in Ni Nanoparticle-Dispersed Multiwalled Carbon Nanotubes. *J. Phys. Chem. B* **2005**, *109*, 8983–8986.
10. Kong, J.; Chapline, M. G.; Dai, H. Functionalized Carbon Nanotubes for Molecular Hydrogen Sensors. *Adv. Mater.* **2001**, *13*, 1384–1386.
11. Sun, Y; Wang, H. H. High-Performance, Flexible Hydrogen Sensors That Use Carbon Nanotubes Decorated with Palladium Nanoparticles. *Adv. Mater.* **2007**, *19*, 2818–2823.
12. Hanson, G. W.; Smith, P. Modeling the Optical Interaction Between a Carbon Nanotube and a Plasmon Resonant Sphere. *IEEE Trans. Antennas Propag.* **2007**, *55*, 3063–3069.
13. Laocharoensuk, R.; Burdick, J.; Wang, J. Carbon-Nanotube-Induced Acceleration of Catalytic Nanomotors. *ACS Nano* **2008**, *2*, 1069–1075.
14. Xue, B.; Chen, P.; Hong, Q.; Lin, J.; Tan, K. L. Growth of Pd, Pt, Ag and Au Nanoparticles on Carbon Nanotubes. *J. Mater. Chem.* **2001**, *11*, 2378–2381.
15. Wang, D.; Li, Z.-C.; Chen, L. Templated Synthesis of Single-Walled Carbon Nanotube and Metal Nanoparticle Assemblies in Solution. *J. Am. Chem. Soc.* **2006**, *128*, 15078–15079.
16. Lordi, V.; Yao, N.; Wei, J. Method for Supporting Platinum on Single-Walled Carbon Nanotubes for a Selective Hydrogenation Catalyst. *Chem. Mater.* **2001**, *13*, 733–737.
17. Quinn, B. M.; Dekker, C.; Lemay, S. G. Electrodeposition of Noble Metal Nanoparticles on Carbon Nanotubes. *J. Am. Chem. Soc.* **2005**, *127*, 6146–6147.
18. Day, T. M.; Unwin, P. R.; Wilson, N. R.; Macpherson, J. V. Electrochemical Templating of Metal Nanoparticles and Nanowires on Single-Walled Carbon Nanotube Networks. *J. Am. Chem. Soc.* **2005**, *127*, 10639–10647.
19. Choi, H. C.; Shim, M.; Bangsaruntip, S.; Dai, H. Spontaneous Reduction of Metal Ions on the Sidewalls of Carbon Nanotubes. *J. Am. Chem. Soc.* **2002**, *124*, 9058–9059.
20. Qu, L.; Dai, L. Substrate-Enhanced Electroless Deposition of Metal Nanoparticles on Carbon Nanotubes. *J. Am. Chem. Soc.* **2005**, *127*, 10806–10807.
21. Qu, L.; Dai, L.; Osawa, E. Shape/Size-Controlled Syntheses of Metal Nanoparticles for Site-Selective Modification of Carbon Nanotubes. *J. Am. Chem. Soc.* **2006**, *128*, 5523–5532.
22. Kim, D. S.; Lee, T.; Geckeler, K. E. Hole-Doped Single-Walled Carbon Nanotubes: Ornamenting with Gold Nanoparticles in Water. *Angew. Chem., Int. Ed.* **2006**, *45*, 104–107.
23. Burda, C.; Chen, X.; Narayanan, R.; El-Sayed, M. A. Chemistry and Properties of Nanocrystals of Different Shapes. *Chem. Rev.* **2005**, *105*, 1025–1102.
24. Wang, Y.; Xia, Y. Bottom-Up and Top-Down Approaches to the Synthesis of Monodispersed Spherical Colloids of Low Melting-Point Metals. *Nano Lett.* **2004**, *4*, 2047–2050.
25. Govindaraj, A.; Vivekchand, S. R. C.; Rao, C. N. R. Novel Vapor Phase Reactions for the Synthesis and Modification of Carbon Nanotubes and Inorganic Nanowires. *J. Nanosci. Nanotechnol.* **2007**, *7*, 1695–1702.
26. Guan, H.; Shao, C.; Wen, S.; Chen, B.; Gong, J.; Yang, X. Preparation and Characterization of NiO Nanofibres *via* an Electrospinning Technique. *Inorg. Chem. Commun.* **2003**, *6*, 1302–1303.
27. Redl, F. X.; Black, C. T.; Papaefthymiou, G. C.; Sandstrom, R. L.; Yin, M.; Zeng, H.; Murray, C. B.; O'Brien, S. P. Magnetic, Electronic, and Structural Characterization of Nonstoichiometric Iron Oxides at the Nanoscale. *J. Am. Chem.Soc.* **2004**, *126*, 14583–14599.
28. Song, R.-Q.; Xu, A.-W.; Deng, B.; Li, Q.; Chen, G.-Y. From Layered Basic Zinc Acetate Nanobelts to Hierarchical Zinc Oxide Nanostructures and Porous Zinc Oxide Nanobelts. *Adv. Funct. Mater.* **2007**, *17*, 296–306.
29. Vovchenko, L.; Matzui, L.; Zakharenko, M.; Babich, M.; Brusilovetz, A. Thermoexfoliated Graphite as Support for Production of Metal−Graphite Nanocomposites. *J. Phys. Chem. Solids* **2004**, *65*, 171–175.
30. Miyawaki, J.; Yudasaka, M.; Imai, H.; Yorimitsu, H.; Isobe, H.; Nakamura, E.; Iijima, S. *In Vivo* Magnetic Resonance Imaging of Single-Walled Carbon Nanohorns by Labeling with Magnetite Nanoparticles. *Adv. Mater.* **2006**, *18*, 1010–1014.
31. Li, Y.; Lee, E. J.; Cho, S. O. Superhydrophobic Coatings on Curved Surfaces Featuring Remarkable Supporting Force. *J. Phys. Chem. C* **2007**, *111*, 14813–14817.
32. Yao, Y.-L.; Ding, Y.; Ye, L.-S.; Xia, X.-H. Two-Step Pyrolysis Process to Synthesize Highly Dispersed Pt-Ru/Carbon Nanotube Catalysts for Methanol Electrooxidation. *Carbon* **2006**, *44*, 61–66.
33. Gu, Y.-J.; Wong, W.-T. Nanostructure PtRu/MWNTs as Anode Catalysts Prepared in a Vacuum for Direct Methanol Oxidation. *Langmuir* **2006**, *22*, 11447–11452.
34. Yung, K.-F.; Wong, W.-T. Synthesis and Catalytic Studies of Uniform Os & Os−Pd Nanoparticles Supported on MWNTs. *J. Cluster Sci.* **2007**, *18*, 51–65.
35. Karousis, N.; Tsotsou, G.-E.; Evangelista, F.; Rudolf, P.; Ragoussis, N.; Tagmatarchis, N. Carbon Nanotubes Decorated with Palladium Nanoparticles: Synthesis, Characterization, and Catalytic Activity. *J. Phys. Chem. C* **2008**, *112*, 13463–13469.
36. A patent application of this method has been filed (USPTO Application No.: 20070292699).
37. Courty, A.; Henry, A.-I.; Pileni, M.-P. Large Triangular Single Crystals Formed by Mild Annealing of Self-Organized Silver Nanocrystals. *Nat. Mater.* **2007**, *6*, 900–907.
38. Lee, H.-H.; Chou, K.-S.; Huang, K.-C. Inkjet Printing of Nanosized Silver Colloids. *Nanotechnology* **2005**, *16*, 2436–2441.

39. Dresselhaus, M. S.; Dresselhaus, G.; Jorio, A.; Souza, A. G.; Samsonidze, G. G.; Saito, R. Science and Applications of Single Nanotube Raman Spectroscopy. *J. Nanosci. Nanotechnol.* **2003**, *3*, 19–37.
40. Kataura, H.; Kumazawa, Y.; Maniwa, Y.; Umezu, I.; Suzuki, S.; Ohtsuka, Y.; Achiba, Y. Optical Properties of Single-Wall Carbon Nanotubes. *Synth. Met.* **1999**, *103*, 2555–2558.
41. Pimenta, M. A.; Marucci, A.; Empedocles, S. A.; Bawendi, M. G.; Hanlon, E. B.; Rao, A. M.; Eklund, P. C.; Smalley, R. E.; Dresselhaus, G.; Dresselhaus, M. S. Raman Modes of Metallic Carbon Nanotubes. *Phys. Rev. B* **1998**, *58*, R16016.
42. Brown, S. D. M.; Jorio, A.; Corio, P.; Dresselhaus, M. S.; Dresselhaus, G.; Saito, R.; Kneipp, K. Origin of the Breit−Wigner−Fano Lineshape of the Tangential G-Band Feature of Metallic Carbon Nanotubes. *Phys. Rev. B* **2001**, *63*, 155414.
43. Rao, A. M.; Eklund, P. C.; Bandown, S.; Thess, A.; Smalley, R. E. Evidence for Charge Transfer in Doped Carbon Nanotube Bundles from Raman Scattering. *Nature* **1997**, *388*, 257–259.
44. Shin, H.-J.; Kim, S. M.; Yoon, S.-M.; Benayad, A.; Kim, K. K.; Kim, S. J.; Park, H. K.; Choi, J.-Y.; Lee, Y. H. Tailoring Electronic Structures of Carbon Nanotubes by Solvent with Electron-Donating and -Withdrawing Groups. *J. Am. Chem. Soc.* **2008**, *130*, 2062–2066.
45. Voggu, R.; Rout, C. S.; Franklin, A. D.; Fisher, T. S.; Rao, C. N. R. Extraordinary Sensitivity of the Electronic Structure and Properties of Single-Walled Carbon Nanotubes to Molecular Charge-Transfer. *J. Phys. Chem. C* **2008**, *112*, 13053–13056.
46. Our results seem to disagree with observations made by Corio, Filho, and co-workers,[47,48] who reported similar BWF line shape diminishment from the encapsulation of CrO_3. The results were opposite when Ag was used. One explanation could be the different sample morphology studied (decorated *vs* filled).
47. Corio, P.; Santos, A. P.; Santos, P. S.; Temperini, M. L. A.; Brar, V. W.; Pimenta, M. A.; Dresselhaus, M. S. Characterization of Single Wall Carbon Nanotubes Filled with Silver and with Chromium Compounds. *Chem. Phys. Lett.* **2004**, *383*, 475–480.
48. Fagan, S. B.; Filho, A. G. S.; Filho, J. M.; Corio, P.; Dresselhaus, M. S. Electronic Properties of Ag- and CrO_3-Filled Single-Walled Carbon Nanotubes. *Chem. Phys. Lett.* **2005**, *406*, 54–59.
49. Subramaniam, C.; Sreeprasad, T. S.; Pradeep, T.; Kumar, G. V. P.; Narayana, C.; Yajima, T.; Tanaka, H.; Ogawa, T.; Chakrabarti, J. Visible Fluorescence Induced by the Metal Semiconductor Transition in Composites of Carbon Nanotubes with Noble Metal Nanoparticles. *Phys. Rev. Lett.* **2007**, *99*, 167404.
50. Kim, K. K.; Bae, J. J.; Park, H. K.; Kim, S. M.; Geng, H.-Z.; Park, K. A.; Shin, H.-J.; Yoon, S.-M.; Benayad, A.; Choi, J.-Y.; Lee, Y. H. Fermi Level Engineering of Single-Walled Carbon Nanotubes by $AuCl_3$ Doping. *J. Am. Chem. Soc.* **2008**, *130*, 12757–12761.
51. Kim, K. K.; Park, J. S.; Kim, S. J.; Geng, H. Z.; An, K. H.; Yang, C.-M.; Sato, K.; Saito, R.; Lee, Y. H. Dependence of Raman Spectra G′ Band Intensity on Metallicity of Single-Wall Carbon Nanotubes. *Phys. Rev. B* **2007**, *76*, 205426.
52. Kalbac, M.; Kavan, L.; Dunsch, L.; Dresselhaus, M. S. Development of the Tangential Mode in the Raman Spectra of SWCNT Bundles during Electrochemical Charging. *Nano Lett.* **2008**, *8*, 1257–1264.
53. Kneipp, K.; Kneipp, H.; Itzkan, I.; Dasari, R. R.; Feld, M. S. Ultrasensitive Chemical Analysis by Raman Spectroscopy. *Chem. Rev.* **1999**, *99*, 2957–2976.
54. Tian, Z.-Q.; Ren, B.; Wu, D.-Y. Surface-Enhanced Raman Scattering: From Noble to Transition Metals and from Rough Surfaces to Ordered Nanostructures. *J. Phys. Chem. B* **2002**, *106*, 9463–9483.
55. Chen, Y.-C.; Young, R. J.; Macpherson, J. V.; Wilson, N. R. Single-Walled Carbon Nanotube Networks Decorated with Silver Nanoparticles: A Novel Graded SERS Substrate. *J. Phys. Chem. C* **2007**, *111*, 16167–16173.
56. Lefrant, S.; Baltog, I.; de la Chapelle, M. L.; Baibarac, M.; Louarn, G.; Journet, C.; Bernier, P. Structural Properties of Some Conducting Polymers and Carbon Nanotubes Investigated by SERS Spectroscopy. *Synth. Met.* **1999**, *100*, 13–27.
57. Kneipp, K.; Kneipp, H.; Corio, P.; Brown, S. D. M.; Shafer, K.; Motz, J.; Perelman, L. T.; Hanlon, E. B.; Marucci, A.; Dresselhaus, G.; Dresselhaus, M. S. Surface-Enhanced and Normal Stokes and Anti-Stokes Raman Spectroscopy of Single-Walled Carbon Nanotubes. *Phys. Rev. Lett.* **2000**, *84*, 3470–3473.
58. Corio, P.; Brown, S. D. M.; Marucci, A.; Pimenta, M. A.; Kneipp, K.; Dresselhaus, G.; Dresselhaus, M. S. Surface-Enhanced Resonant Raman Spectroscopy of Single-Wall Carbon Nanotubes Adsorbed on Silver and Gold Surfaces. *Phys. Rev. B* **2000**, *61*, 13202–13211.
59. Fantini, C.; Jorio, A.; Souza, M.; Saito, R.; Samsonidze, G. G.; Dresselhaus, M. S.; Pimenta, M. A. Steplike Dispersion of the Intermediate-Frequency Raman Modes in Semiconducting and Metallic Carbon Nanotubes. *Phys. Rev. B* **2005**, *72*, 085446.
60. Fantini, C; Pimenta, M. A.; Strano, M. S. Two-Phonon Combination Raman Modes in Covalently Functionalized Single-Wall Carbon Nanotubes. *J. Phys. Chem. C* **2008**, *112*, 13150–13155.
61. Zhang, X.; Zhang, W.; Liu, L.; Shen, Z. X. Surface-Enhanced Raman of Z-Vibration Mode in Single-Walled and Multi-Walled Carbon Nanotube. *Chem. Phys. Lett.* **2003**, *372*, 497–502.
62. Li, Y. B.; Wei, B. Q.; Liang, J.; Yu, Q.; Wu, D. H. Transformation of Carbon Nanotubes to Nanoparticles by Ball Milling Process. *Carbon* **1999**, *37*, 493–497.
63. Pierard, N.; Fonseca, A.; Konya, Z.; Willems, I.; Tendeloo, G. V.; Nagy, J. B. Production of Short Carbon Nanotubes with Open Tips by Ball Milling. *Chem. Phys. Lett.* **2001**, *335*, 1–8.
64. Liu, F.; Zhang, X.; Cheng, J.; Tu, J.; Kong, F.; Huang, W.; Chen, C. Preparation of Short Carbon Nanotubes by Mechanical Ball Milling and Their Hydrogen Adsorption Behavior. *Carbon* **2003**, *41*, 2527–2532.
65. Mulvaney, P. Surface Plasmon Spectroscopy of Nanosized Metal Particles. *Langmuir* **1996**, *12*, 788–800.
66. Doering, W.; Piotti, M. E.; Natan, M. J.; Freeman, R. G. SERS as a Foundation for Nanoscale, Optically Detected Biological Labels. *Adv. Mater.* **2007**, *19*, 3100–3108.
67. Itkis, M. E.; Niyogi, S.; Meng, M.; Hamon, M. A.; Hu, H.; Haddon, R. C. Spectroscopic Study of the Fermi Level Electronic Structure of Single-Walled Carbon Nanotubes. *Nano Lett.* **2002**, *2*, 155–159.
68. The salt-to-metal conversion could occur during the ball-milling process even without any subsequent thermal treatment (to be reported separately).
69. Yu, R.; Chen, L.; Liu, Q.; Lin, J.; Tan, K.-L.; Ng, S. C.; Chan, H. S. O.; Xu, G.-Q.; Hor, T. S. A. Platinum Deposition on Carbon Nanotubes *via* Chemical Modification. *Chem. Mater.* **1998**, *10*, 718–722.
70. Bond, A. M.; Miao, W.; Raston, C. L. Mercury(II) Immobilized on Carbon Nanotubes: Synthesis, Characterization, and Redox Properties. *Langmuir* **2000**, *16*, 6004–6012.
71. There are several recent reports on the metal or metal oxide decoration on graphene sheets *via* solution methods.[72−75]
72. Muszynski, R.; Seger, B.; Kamat, P. V. Decorating Graphene Sheets with Gold Nanoparticles. *J. Phys. Chem. C* **2008**, *112*, 5263–5266.
73. Williams, G.; Seger, B.; Kamat, P. V. TiO_2-Graphene Nanocomposites. UV-Assisted Photocatalytic Reduction of Graphene Oxide. *ACS Nano* **2008**, *2*, 1487–1491.
74. Yuge, R.; Zhang, M.; Tomonari, M.; Yoshitake, T.; Iijima, S.; Yudasaka, M. Site Identification of Carboxyl Groups on Graphene Edges with Pt Derivatives. *ACS Nano* **2008**, *2*, 1865–1870.
75. Lu, J.; Do, I.; Drzal, L. T.; Worden, R. M.; Lee, I. Nanometal-Decorated Exfoliated Graphite Nanoplatelet Based

Glucose Biosensors with High Sensitivity and Fast Response. *ACS Nano* **2008**, *2*, 1825–1832.
76. The use of a platinum acetate compound (City Chemicals; containing ~5 wt % Ag impurity) with MWCNT yielded a nanohybrid in which the nanotubes were decorated with narrowly distributed metal nanoparticles of 2−3 nm in diameter (see Figure S7 in Supporting Information). The use of some non-acetate organic (such as platinum(II) acetylacetonate) or inorganic compounds (such as $H_2Pt(OH)_6$, $HAuCl_4$, AuI, and $RuCl_3$) in similar processes was also successful, yielding carbon nanotubes decorated with the corresponding 0-valence metal nanoparticles of various sizes.
77. Judd, M. D.; Plunkett, B. A.; Pope, M. I. The Thermal Decomposition of Calcium, Sodium, Silver and Copper(II) Acetates. *J. Therm. Anal.* **1974**, *6*, 555–563.
78. Gallagher, P. K.; Gross, M. E. The Thermal Decomposition of Palladium Acetate. *J. Therm. Anal.* **1986**, *31*, 1231–1241.
79. Pol, S. V.; Pol, V. G.; Felner, I.; Gedanken, A. The Thermal Decomposition of Three Magnetic Acetates at Their Autogenic Pressure Yields Different Products. Why? *Eur. J. Inorg. Chem.* **2007**, 2089–2096.
80. Logvinenko, V.; Polunina, O.; Mikhailov, Y.; Mikhailov, K.; Bokhonov, B. Study of Thermal Decomposition of Silver Acetate. *J. Therm. Anal. Calorim.* **2007**, *90*, 813–816.
81. Šljukić, B.; Banks, C. E.; Crossley, A.; Compton, R. G. Copper Oxide−Graphite Composite Electrodes: Application to Nitrite Sensing. *Electroanal.* **2007**, *19*, 79–84.
82. Langley, C. E.; Šljukić, B.; Banks, C. E.; Compton, R. G. Manganese Dioxide Graphite Composite Electrodes: Application to the Electroanalysis of Hydrogen Peroxide, Ascorbic Acid and Nitrite. *Anal. Sci.* **2007**, *23*, 165–170.
83. Šljukić, B.; Banks, C. E.; Crossley, A.; Compton, R. G. Lead(IV) Oxide−Graphite Composite Electrodes: Application to Sensing of Ammonia, Nitrite and Phenols. *Anal. Chim. Acta* **2007**, *587*, 240–246.
84. Ebbesen, T. W.; Hiura, H.; Bisher, M. E.; Treacy, M. M. J.; Shreeve-Keyer, J. L.; Haushalter, R. C. Decoration of Carbon Nanotubes. *Adv. Mater.* **1996**, *8*, 155–157.
85. Ebbesen, T. W. Wetting, Filling and Decorating Carbon Nanotubes. *J. Phys. Chem. Solids* **1996**, *57*, 951–955.
86. Lineberry, Q. J.; Cao, Y.; Lin, Y.; Ghose, S.; Connell, J. W.; Pan, W.-P. Mercury Capture from Flue Gas Using Palladium Nanoparticle-Decorated Substrates as Injected Sorbents. *Energy Fuels*, DOI: 10.1021/ef800733h.
87. A patent application has been filed (USPTO Application No.: 20090022977).